Rotational Structure of Small ^{4}He Clusters Seeded with HF, HCl, and HBr Molecules†

Jordan A. Ramilowski, Aleksandra A. Mikosz, and David Farrelly*

Department of Chemistry and Biochemistry, Utah State University, Logan, Utah 84322-0300

José Luis Cagide Fajín and Berta Fernández

Faculty of Chemistry, Department of Physical Chemistry, University of Santiago de Compostela, E-15782 Santiago de Compostela, Spain

Received: June 14, 2007; In Final Form: July 25, 2007

Diffusion Monte Carlo calculations are performed for ground and excited rotational states of $HX(^4He)_N$, complexes with $N \leq 20$ and $X = F$, Cl, Br. The calculations are done using ab initio He−HX intermolecular potentials whose computation is described. Intermolecular energies and He radial and angular probability density distributions are computed as a function of the number of solvent atoms. Excited states are calculated using fixed-node diffusion Monte Carlo methods, and molecule-solvent angular momentum coupling is studied as a function of cluster size and potential anisotropy. Nodal surfaces of the many-body wave function are computed approximately by making an adiabatic Born−Oppenheimer-like separation of radial and angular degrees of freedom of the cluster. This procedure is extended to include radial dependencies in the adiabatic nodal function. We predict that the observed decrease in the gas-phase rotational constants for HCl and HBr in a ^{4}He nanodroplet will be smaller than that observed for HF, despite HF's having the largest (by far) gas-phase rotational constant of the three molecules. This suggests that the specifics of the solvation dynamics of a molecule in a ^{4}He cluster are the result of a delicate interplay between the magnitude of the gas-phase rotational constant of the molecule and the anisotropic contributions to the atom−molecule potential energy.

1. Introduction

Helium is a substance with singular properties; it has no triple point and so is the only material known that can exist as a liquid at absolute zero;[1−4] below 2.17 K, helium-4 behaves as a superfluid but is not a pure Bose condensate;[5] liquid helium-4 has a thermal conductivity ≈30 times greater than copper;[1,2,6] it apparently has a supersolid phase;[7−10] the ^{4}He dimer is renowned for its small binding energy[11] (≈1 mK) and large bond length[11] ($\langle r \rangle \approx 100$ bohr); and $^4He_3$ has been predicted to exhibit an Efimov state.[12,13] In contrast, fermionic helium-3 does not achieve superfluidity until 0.0025 K, and bound states of the dimer and trimer do not exist at all because of the higher zero-point energy of ^3He_N clusters.[4,14] The threshold for the appearance of ^3He_N droplets is likely to be in the range $20 < N < 40$.[14,15]

The peculiarities of the properties of helium are only exaggerated by confining the geometry of the system, for example, as in a film or droplet.[6,14,16,17] Due to the very weak He−He interaction, He droplets containing $\approx 10^3-10^8$ atoms cool down very efficiently by evaporation and achieve temperatures of 0.37 K (^{4}He) and 0.15 K (^{3}He) in a free jet expansion.[6,16,18] Consequently, droplets of ^{4}He are superfluid, whereas those of ^{3} He behave as conventional liquids.[6,14] Nanodroplets of ^{4}He have been called the "ultimate spectroscopic matrix"[19] but they also offer potential as ultracold,[20] ultraclean nanoreactors;[6] for example, for making and characterizing novel chemical species,[18] performing high-resolution spectroscopy of van der Waals complexes,[21,22] studying or creating complexes of biomolecules,[6,23] monitoring chemical reactions between individual molecules,[6] isolating reaction intermediates or precursors,[24] and studying the onset and nature of superfluidity in finite-sized systems.[25,26] Several comprehensive reviews of the field exist.[6,14,16,27−30]

The utility of ^{4}He droplets can be traced in part to their superfluid nature and in part to the efficiency of evaporative cooling as the droplet expels atoms.[6,14] Consider, for example, the formation of molecular clusters. In a typical free jet expansion, cluster formation occurs early in the expansion and is followed by relatively slow cooling through two-body collisions. The opposite happens in a ^{4}He droplet experiment. There, the droplet picks up molecules sequentially (according to Poisson statistics[16,31,32]), with the average time between capture events greatly exceeding the time needed for each molecule to cool through evaporation of He atoms from the droplet. Thus, in a droplet, molecular clusters are built from already cold molecules, and this can produce novel arrangements, for example, linear chains of HCN molecules oriented by long-range dipole−dipole interactions.[18] This procedure rather neatly avoids the usual problem of rotational motion swamping dipole−dipole interactions. In other (actual or prospective) applications, molecules seeded into nanodroplets can serve as antennae with which to relay information to and from the droplet; for example, structural information about species being formed in the droplet[33] or information about the onset of superfluidity as a function of droplet size.[25,26,34]

Indications of the utility of ^{4}He droplets as ultragentle cryogenic matrixes were apparent even in pioneering spectroscopic studies: in 1992 Goyal et al.[35] observed unusually narrow absorption line widths in SF_6-seeded nanodroplets. This work was followed by high-resolution infrared (IR) studies by

† Part of the "Giacinto Scoles Festschrift".

10.1021/jp0746143 CCC: $37.00
Published on Web 10/11/2007

Hartmann et al.,[36] who observed rovibrational fine structure more typical of gas- than liquid-phase spectra. Although it is exceptional for a molecule dissolved in a liquid to present rotationally resolved lines (HF being one exception[37]) in a ^{4}He nanodroplet, coherent free rotation over many periods appears to be the norm.[16] Still, the liquid- and gas-phase spectra are not identical: in most cases, the spectroscopic constants of the solvated molecule are shifted from their gas-phase values. For example, SF_6 in a ^{4}He nanodroplet exhibits a spherical top spectrum but with a rotational constant, B, approximately one-third of B_0, its gas-phase value.[36]

The first calculations of the rotational structure of a molecule in a ^{4}He cluster were diffusion Monte Carlo (DMC) simulations for $SF_6(^4He)_N$ clusters.[38] From these calculations, it emerged that a fraction of the helium density in the droplet follows the rotation of the SF_6 molecule adiabatically. In the "adiabatic following" model that resulted from these calculations, the observed decrease in the rotational constant is due to the molecule's dragging a fraction of the helium density along as it rotates, thereby increasing its moment of inertia.

A good definition of quantum solvation is that dissolved molecules are coated by a solvation shell, and at some point, as a function of the number of solvent atoms, angular momentum coupling with the solvent atoms saturates. This situation then allows for apparent free rotational motion, albeit with altered spectroscopic constants.[14,38−40] Recently, this has been studied in more detail in experiments that effectively build up the quantum solvent He atom by He atom; more precisely, clusters containing specific numbers of He atoms (e.g., from 1 to 20) can be individually interrogated.[40−43] It turns out that the transition from a "molecular complex" to a "dissolved molecule" can occur for as few as ≈7−12 ^{4}He atoms. Various simulations of the onset of solvation have been made,[38,40,44−47] yet the underlying physical mechanism for this transition continues to be a subject of active research.[6,39,40,47]

Because the experiments are conducted at ultralow temperatures, only the lowest rotational excited states are typically accessed. However, although this simplifies simulations, the many-body nature of the system rules out most computational procedures. Diffusion Monte Carlo methods are one exception and, in fact, are ideal for computing accurate ground state energies for very large systems with high accuracy. However, DMC suffers from the drawback that the calculation of excited states is not straightforward, and approximations must usually be introduced. The situation is alleviated somewhat by the observation that experiments involve only the lowest-lying excited states. One approach for computing excited states is fixed-node DMC, in which knowledge of the nodal topology of the wave function is built into the simulations. The nodal topology of the excited state being sought after can sometimes be obtained using known symmetries of the system. For many-body molecule−^4He_N clusters, however, it is necessary to resort to approximations. A new approach to computing nodes has recently been developed in which estimates of nodal surfaces are obtained using a Born−Oppenheimer-like separation of radial and angular motions.[47,48] This approach, called adiabatic-node-diffusion Monte Carlo (ANDMC), was applied to the quantum solvation of HCN in a small helium-4 droplet.[47] For the binary He−HX complexes considered in this article, we will utilize ANDMC, and a direct comparison will be made between adiabatic and accurate nodal topologies.

In ANDMC, radial and angular motions are separated, and the resulting angular Hamiltonian is then diagonalized to yield estimates for nodal topologies of the many-body wave function. Using this method, accurate excited-state rotational energies were calculated for $HCN(^4He)_N$ droplets. The adiabatic node approach also has the advantage that it allows the mechanics of angular momentum coupling (and decoupling) between identical bosons and the molecular rotor to be mapped out explicitly. For $HCN(^4He)_N$ complexes it was found that, for small values of N, there exists significant angular momentum coupling between the molecule and the helium atoms. However, because of the bosonic symmetry requirement on the wave function, as N is increased and solvation becomes almost complete, the degree of atom−molecule angular momentum coupling saturates. In particular, for the HCN system, the details of angular momentum coupling and decoupling were related to (i) the angular anisotropy of the potential energy surface (PES); for example, which Legendre polynomials contribute to the PES in an expansion of the angular coordinates; and (ii) the size of the rotational constant of the gas-phase molecule.

The reasons why and how these factors are expected to affect the solvation dynamics can be understood by thinking of seeded ^{4}He clusters as being bosonic "superatoms". Imagine that the molecular rotor has infinite mass and the atom−molecule potential is isotropic. In this limit, the Hamiltonian is essentially that of an atom except that the "electrons", that is, the ^{4}He atoms, are bosons, and the form of the "electron−electron" interaction is quite different from a real atom. Neglecting He−He interactions results in a rough analog of an atom in the central-field approximation but with bosonic "electrons". This model has few computational merits (although it is a useful limit to use in tests of algorithms) but it does bring into focus the importance of understanding angular momentum coupling in a seeded ^{4}He cluster. This is entirely analogous to how angular momentum coupling is central to understanding electronic structure.[49]

In the actual physical situation, anisotropies of the interaction potential couple rotational states of the molecule with the orbital angular momenta of the He atoms. This is in addition to the smaller couplings between He atoms due to the He−He interaction potential and to He−molecule−He interactions, etc. However, the He−molecule couplings will also be modulated by the size of the gas-phase rotational constant. As was shown in an earlier study of SF_6,[38] artificially increasing the gas-phase rotational constant tends to decouple the molecule adiabatically from the He atoms and the system effectively behaves increasingly as if the PES were more isotropic. In general, the details of quantum solvation are, therefore, expected to depend on the competition between large B_0 values, which tend to enhance the effective decoupling of the molecule and the solvent, and large potential anisotropies, which tend to increase the effective coupling. The current study is directed to quantifying the importance of these factors by studying clusters seeded with HF, HCl, and HBr molecules. The vibrational frequency shift in helium clusters was studied experimentally and theoretically, using the DMC methods by Blume et al.[50]

In recent work, Paolini et al.[40] investigated the convergence of the apparent rotational constant of a molecule seeded into a ^{4}He cluster as a function of cluster size. They found that for HCN seedants, the effective rotational constant did not change significantly beyond $N \sim 15$. This is similar to the case of CO[51] and is also in agreement with high-resolution IR spectra recently obtained for He clusters seeded with CO.[43,52] However, these results differed from earlier expectations of relatively slow convergence to the nanodroplet limit for light rotors.[53]

To understand further the relative roles of the size of the gas-phase rotational constant and the strength and anisotropy of the He molecule interaction potential, Paolini et al.[40] performed

computations of the solvation of two so-called "fudged" molecules *f*-OCS and *f*-HCN; that is, OCS and HCN in which artificially small or large values of the gas-phase rotational constant were used. This approach is similar to that employed in the earlier study of SF_6.[38] They concluded that it is the strength and anisotropy of the He−molecule interaction, rather than B_0, that is mainly responsible for the reduction of the rotational constant in the nanodroplet regime. Therefore, the common classification of molecular dopants in ^{4}He clusters into "heavy" and "light" rotors seems to rely upon a coincidence: heavier molecules tend to have stronger and more anisotropic interactions with He.[40]

To clarify the competing roles of B_0 and the potential anisotropy further, ANDMC was used[47] to trace the saturation of the bosonic solvent and solute angular wave functions in HCN-seeded clusters. Convergence of the effective rotational constant to its asymptotic limit (as a function of cluster size) was explained in terms of the specific anisotropic contributions to the interaction potential that lead to specific couplings between angular momentum basis vectors. It was also shown that adiabatic nodes substantially improve DMC estimates in this system. This allowed a mechanism to be put forward to explain the observed convergence of the *a*-series of lines observed experimentally to the nanodroplet limit as well as the sudden disappearance of the *b*-series.[47] Although the ultimate explanation for the vanishing of the *b*-series was similar to that proposed in other studies,[51,54] it was arrived at differently: the mechanism was couched explicitly in terms of angular momentum coupling arguments. Similar behavior is expected for CO-seeded clusters, since the CO−He and HCN−He interaction potentials are similar, as are the molecular constants.[52]

Rather than using fudged molecules, in the current study, the solvation dynamics of the three molecules (HF, HCl and HBr) are studied. The molecules have rather different gas-phase rotational constants, and the interaction potentials differ in several subtle but significant ways. An aim of the study is to test how good variously proposed rules of thumb, for example, "light-rotor" versus "heavy-rotor",[40] are at predicting system properties. It might, for example, be expected that HF, having the largest B_0 value, will on solvation exhibit the smallest reduction in rotational constant of the three molecules. Although several potential energy surfaces for He−HX (X = F, Cl, Br) already exist in the literature,[55−59] to make a more consistent and even-handed comparison, ab initio PESs for all three complexes are computed and fitted to the same functional form. We find that (i) it is not only the size of the anisotropy that matters but also its symmetry; that is, which Legendre polynomials contribute to the angular anisotropy; and (ii) the bosonic symmetry of the solvent requires that all of the He atoms couple identically to the molecule. Eventually, the coupling of the atom and molecular angular momentum saturates and the molecule solvates.[47]

The paper is organized as follows: the Hamiltonian is introduced in Section 2. Details of the calculation of the intermolecular PESs are also provided in Section 2, together with the parameters and functions used in an analytical fit to each surface. The energies of the binary He−HX complexes are computed in Section 3 using coupled-channel and diagonalization methods. Comparison is also made with DMC results. Details of the DMC approach are contained in Section 4. In Section 5, He radial and angular density probability distributions are computed as a function of cluster size. Rotational excited-state DMC calculations are presented in Section 6. Conclusions are in Section 7.

TABLE 1: Atomic and Molecular Masses and Molecular Rotational Constants[61,62]

atom/molecule	mass (a.m.u.)	rotational constant (cm^{-1})
^{4}He	4.002 60	
HF	20.006 34	20.560
HCl	36.460 94	10.403
HBr	80.911 94	8.473

TABLE 2: Parameters of the Analytical PES Fitted to the ab Initio Interaction Energies of the He−HF Complex[a]

parameter	value	parameter	value
C_6^0	−0.014 012 380 008 63	g_{05}	−0.025 168 817 8 45 84
C_6^2	0.007 937 515 978 14	g_{10}	−3.732 350 583 153 67
b_0	13.351 403 472 923 70	g_{11}	−0.488 757 370 932 63
b_1	−0.090 562 572 509 10	g_{12}	−0.662 023 973 510 30
b_2	0.362 226 204 951 96	g_{13}	−0.611 875 129 971 62
b_3	0.107 520 256 279 37	g_{14}	−0.199 329 101 137 73
b_4	−0.107 290 933 956 87	g_{15}	0.027 440 366 871 53
b_5	0.098 674 150 965 43	g_{20}	1.043 244 478 915 95
d_0	−2.531 461 160 701 42	g_{21}	0.094 027 724 972 21
d_1	0.074 212 679 748 84	g_{22}	0.201 717 781 047 36
d_2	−0.082 760 716 288 34	g_{23}	0.162 295 782 259 88
d_3	−0.014 989 938 940 00	g_{24}	0.037 857 162 445 61
d_4	0.043 300 762 412 91	g_{25}	−0.006 465 746 084 38
d_5	−0.038 020 786 066 27	g_{30}	−0.104 414 332 536 13
g_{00}	4.571 863 773 811 32	g_{31}	−0.004 973 155 718 33
g_{01}	0.753 616 111 944 33	g_{32}	−0.021 530 637 619 04
g_{02}	0.721 394 543 773 71	g_{33}	−0.015 006 582 707 22
g_{03}	0.782 715 129 134 56	g_{34}	−0.001 450 529 992 00
g_{04}	0.296 695 427 359 75	g_{35}	0.000 000 000 000 00

[a] This set of parameters requires distances (R) to be in Å and will result in potential values in cm^{-1}. For HF−He $C_7^1 = C_7^3 = 0$.

2. Hamiltonian and Intermolecular Potentials

In the space-fixed frame, the Hamiltonian for N helium atoms interacting with an HX molecule (treated as a linear rigid rotor) is

$$H = \frac{-\hbar^2}{2M}\nabla_I^2 - \frac{\hbar^2}{2m}\sum_{i=1}^{N}\nabla_i^2 + B_0\,\mathbf{j}^2 + \sum_{i<j}^{N} V_{\mathrm{He}}^{\mathrm{He}}(r_{ij}) + \sum_{i=1}^{N} V(R_{iI}, \theta_{iI}) \quad (1)$$

where r_{ij} and R_{iI} denote He−He and He−HX separations, respectively; θ_{iI} is the angle between the molecular axis and the ith He atom (in the case of the dimer complex, HX−He, $\theta_{1I} \rightarrow \theta$); M and m are the masses of the HX molecule and the He atom, respectively; and $V_{\mathrm{He}}^{\mathrm{He}}(r_{ij})$ and $V(R_{iI}, \theta_{iI})$ are the He−He[60] and the HX−He PESs, respectively. The molecular rotational angular momentum operator is $\mathbf{j}$, and B_0 is the gas-phase rotational constant. The various physical constants are collected together in Table 1.[61,62] All calculations are performed in the rigid-body approximation.

2.1. Potential Energy Surfaces. All the calculations to be described assume pairwise molecule−He and He−He interaction potentials. For the He−He interaction, the potential energy surface of Aziz et al. was used.[60] The potential is simply a function of the distance between any two He atoms. Ab initio PESs of the three He−HX van der Waals complexes were calculated directly. The He−HF PES has been reported elsewhere, along with details of the approach taken, but for completeness, the parameters for the HF−He PES are also provided herein.[59] Essentially, the three PESs were obtained by fitting a considerable number of interaction energies obtained at the Coupled Cluster Singles and Doubles levels, including

connected triple corrections. This was done using the augmented correlation consistent polarized valence quintuple zeta (He−HF and He−HCl) and the SDB-aug-cc-pVQZ (He−HBr) basis sets extended with a set of 3*s*3*p*2*d*1*f*1*g* midbond functions. These basis sets were selected after systematic studies carried out at representative intermolecular geometries. Basis set superposition error was corrected for using the counterpoise method of Boys and Bernardi.[63,64]

The potentials are each found to be characterized by two minima corresponding to linear configurations, that is, He−HX and He−XH. The ab initio single-point interaction energies were then fitted to the analytical function $V(R, \theta)$ originally suggested by Bukowski et al.[65] Here, $R = |\mathbf{R}|$ is the distance from the He atom to the molecular center of mass (com), and θ is the angle between **R** and the molecular axis; $\theta = 0$ and $\theta = \pi$ correspond to the linear He−HX and He−XH configurations, respectively. The potential energy function is the sum of two terms: a short-range term, V_{sh}, and an asymptotic term, V_{as}:

$$V(R, \theta) = V_{sh}(R, \theta) + V_{as}(R, \theta) \tag{2}$$

where

$$V_{sh}(R, \theta) = G(R, \theta)e^{B(\theta)+D(\theta)R} \tag{3}$$

and

$$V_{as}(R, \theta) = \sum_{n=6}^{7} \sum_{l}^{n-4}{}' f_n(D(\theta)R) \times \frac{C_n^l}{R^n} P_l(\cos\theta) \tag{4}$$

For HF and HCl, $n = 6$, whereas for HBr, $n = 6, 7$. The Σ' notation means that $l = 0, 2$ (n odd) or $l = 1, 3$ (n odd). The functions $D(\theta)$, $B(\theta)$, and $G(R, \theta)$ are represented as expansions in Legendre polynomials, $P_l(\cos\theta)$:

$$B(\theta) = \sum_{l=0}^{5} b_l P_l(\cos\theta) \tag{5}$$

$$D(\theta) = \sum_{l=0}^{5} d_l P_l(\cos\theta) \tag{6}$$

$$G(R, \theta) = \sum_{l=0}^{5} (g_{0l} + g_{1l}R + g_{2l}R^2 + g_{3l}R^3)P_l(\cos\theta) \tag{7}$$

and

$$f_n(x) = 1 - e^x \sum_{k=0}^{n} \frac{|x|^k}{k!} \tag{8}$$

is a Tang−Toennies damping function[66] with $x = R \times D(\theta)$; b_l, d_l, g_{kl}, and the C_n^l parameters are all adjustable. The fitted values of the corresponding PES parameters are presented in Tables 2−4.The three resulting PESs are shown in Figure 1. Table 5 provides the locations and well depths of the two minima for each complex. Several observations can be made. As the halogen atom increases in size, the He−HX minimum becomes shallower and moves farther out. Essentially, the complex is becoming more spherically symmetric as the halogen atom increases in radius. This observation can be made more quantitative by expanding the PES in Legendre polynomials, that is,

$$V(R, \theta) = \sum_{\lambda} v_\lambda(R)P_\lambda(\cos\theta) \tag{9}$$

Several of the lowest order radial strength functions,[67] $v_\lambda(R)$, are plotted in Figure 2 for each of the three binary complexes. It is readily apparent that the contributions of v_1, v_2, and v_3 decrease relative to v_0 as one goes from HF to HCl to HBr. This observation will prove useful for understanding the excited-state dynamics of these molecules in small ^{4}He clusters.

It is also notable that the deeper minimum corresponds to the He−HF geometry in the He−HF complex but to He−BrH in the He−HBr dimer. The He−HCl complex falls between, with both minima having rather similar binding energies, although the He−ClH well is slightly the deeper of the two.

TABLE 3: Parameters of the Analytical PES Fitted to the ab Initio Interaction Energies of the He−HCl Complex[a]

parameter	value	parameter	value
C_6^0	−0.005 663 57	g_{05}	0.179 848 21
C_6^2	−0.003 130 99	g_{10}	−2.922 571 12
b_0	13.320 102 38	g_{11}	0.251 622 54
b_1	0.342 867 92	g_{12}	−1.216 604 66
b_2	0.298 163 63	g_{13}	−0.111 491 31
b_3	0.294 258 22	g_{14}	−0.267 531 61
b_4	−0.009 346 84	g_{15}	−0.082 111 05
b_5	−0.035 407 20	g_{20}	0.682 127 33
d_0	−2.100 893 30	g_{21}	−0.082 455 50
d_1	0.010 233 81	g_{22}	0.311 774 58
d_2	−0.128 177 19	g_{23}	0.000 000 00
d_3	−0.010 815 82	g_{24}	0.059 213 84
d_4	0.020 431 70	g_{25}	0.009 554 25
d_5	0.006 983 61	g_{30}	−0.055 985 98
g_{00}	4.227 609 10	g_{31}	0.008 917 02
g_{01}	−0.224 386 73	g_{32}	−0.027 760 35
g_{02}	1.588 864 95	g_{33}	0.002 509 68
g_{03}	0.318 829 07	g_{34}	−0.004 349 89
g_{04}	0.396 856 27	g_{35}	0.000 000 000

[a] This set of parameters requires distances (R) to be in Å and will result in potential values in cm^{-1}. For HCl−He, $C_7^1 = C_7^3 = 0$.

TABLE 4: Parameters of the Analytical PES Fitted to the ab Initio Interaction Energies of the He−HBr Complex[a]

parameter	value	parameter	value
C_6^0	−425.239 879 082 69 6	g_{04}	0.557 309 473 281
C_6^2	−320.525 651 759 54 2	g_{05}	−0.076 662 339 377
C_7^1	23.467 575 642 035	g_{10}	−2.879 668 513 147
C_7^3	29.052 464 149 358	g_{11}	0.031 420 907 580
b_0	13.389 610 799 159	g_{12}	0.746 535 010 188
b_1	0.524 091 825 535	g_{13}	−0.531 871 910 461
b_2	0.851 082 514 198	g_{14}	−0.345 678 532 980
b_3	0.280 259 558 185	g_{15}	0.090 918 816 992
b_4	0.275 185 409 402	g_{20}	0.637 568 549 808
b_5	−0.224 208 308 256	g_{21}	−0.020 484 094 623
d_0	−2.039 697 201 455	g_{22}	−0.148 746 579 592
d_1	−0.029 313 071 712	g_{23}	0.103 244 893 893
d_2	−0.093 216 954 967	g_{24}	0.075 891 728 285
d_3	−0.027 635 075 041	g_{25}	−0.031 802 305 582
d_4	−0.064 847 358 666	g_{30}	−0.049 851 078 574
d_5	0.062 929 310 818	g_{31}	0.002 751 241 046
g_{00}	4.404 601 847 646	g_{32}	0.010 627 371 755
g_{01}	0.050 846 483 162	g_{33}	−0.006 629 026 827
g_{02}	−1.270 755 306 096	g_{34}	−0.006 071 430 979
g_{03}	0.912 749 039 267	g_{35}	0.003 520 180 843

[a] This set of parameters requires distances (R) to be in Å and will result in potential values in cm^{-1}.

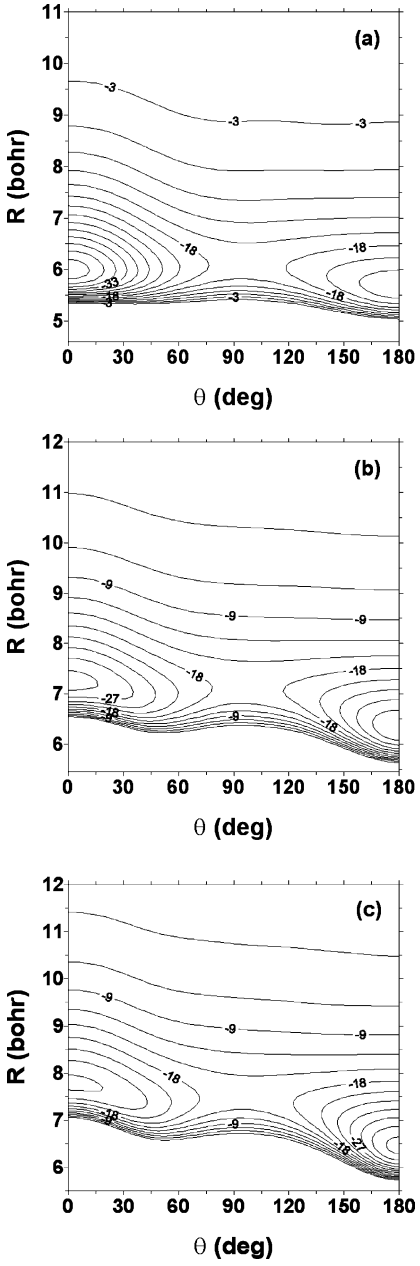

Figure 1. Contour plots of the potential energy surfaces (a) He−HF, (b) He−HCl, (c) He−HBr. θ is the angle between the molecular axis and a vector connecting the com of the molecule and the helium atom. The H atom lies along the positive *z*-axis; that is, $\theta = 0°$ for He−HF and $\theta = 180°$ for He−FH.

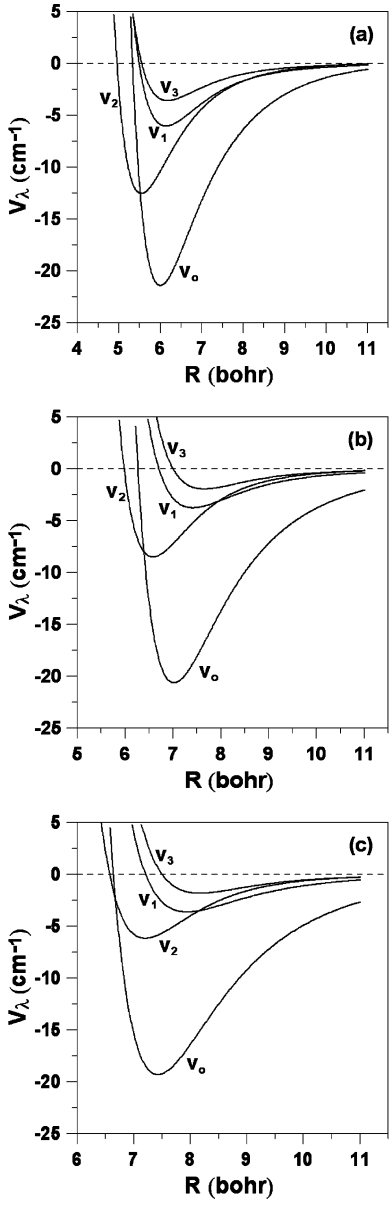

Figure 2. Radial strength (expansion) functions for (a) He−HF, (b) He−HCl, (c) He−HBr PES. As one moves from HF (a) to HBr (c), the relative importance of the v_2 term decreases. *R* is the distance of He atom to the com of the molecule.

TABLE 5: Well Depths and Atom−Molecule Separations at the Two Minima in the Three Dimer PESs[a]

dimer	θ (deg)	R (bohr)	V (cm^{-1})
He−HF	0.0*	5.983*	−43.844*
	180.0	5.667	−26.169
He−HCl	180.0*	6.340*	−32.736*
	0.0	7.242	−31.160
He−HBr	180.0*	6.446*	−37.103*
	0.0	7.783	−27.666

[a] (∗) signifies the global minimum.

3. Energy Levels of the HX−He Binary Complexes

Before proceeding to study droplets containing more than one He atom, it is essential to understand the level structure and the nodal topology of the wave function of the binary complex. This is achieved by using (a) coupled channel calculations[68] and, so as to obtain accurate wave functions and nodal surfaces, (b) matrix diagonalization using a product basis of radial × $|jlJM\rangle$ basis vectors, where *j*, *l*, and *J* are the rotor, atom, and total angular momentum quantum numbers, respectively, and *M* is the projection of the total angular momentum on the space-fixed *z*-axis.[67,69]

First, it is useful to consider a particular limit, the "isotropic binary complex" (IBC): If the molecule−^{4}He interaction potential is isotropic, then the molecular rotational angular momentum and the atomic orbital angular momentum quantum numbers, *j* and *l*, respectively, are separately conserved, that is, for the IBC, the labeling scheme $|jlJ\rangle$ is exact, and the wave function is separable; the molecular and atomic parts of the wave function are spherical harmonics involving the spherical polar angles in the space-fixed frame. The IBC is used to define our working set of basis vectors.

Of particular interest, both theoretically and experimentally, are the nodal functions of the lowest-lying rotational states, for example, levels with $J = 1$, for which the nodal surfaces of the IBC states of most interest, $|011\rangle$ and $|101\rangle$, are $\Psi_{iso}^{(a)} = \cos\theta_2$

TABLE 6: Ground and Excited-State Energies for the He−HF Dimer in cm^{-1}[a]

dominant $\|jlJ\rangle$	CC	D	DMC[1]	DMC[2]	DMC[3]
$\|000\rangle$	−6.718	−6.723	−6.720 ± 0.033	−6.720 ± 0.033	−6.720 ± 0.033
$\|011\rangle$	−5.967	−5.974	−5.987 ± 0.053		
$\|101\rangle$	33.951	33.980	32.392 ± 0.117	32.776 ± 0.107	33.569 ± 0.142
$\|111\rangle$	36.758	36.755			
$\|121\rangle$	37.148	37.144			

[a] CC: coupled channel.[68] D: matrix diagonalization. DMC: fixed-node DMC using [1]the appropriate IBC node, [2]adiabatic, and [3]accurate nodal functions. The $|jlJ\rangle$ labeling scheme is exact only for the isotropic binary complex.

TABLE 7: Ground and Excited-State Energies for the He−HCl Dimer in cm^{-1}[a]

dominant $\|jlJ\rangle$	CC	D	DMC[1]	DMC[2]	DMC[3]
$\|000\rangle$	−7.753	−7.761	−7.748 ± 0.033	−7.748 ± 0.033	−7.748 ± 0.033
$\|011\rangle$	−7.214	−7.213	−7.206 ± 0.041		
$\|101\rangle$	12.765	12.805	12.328 ± 0.057	13.526 ± 0.057	12.505 ± 0.061
$\|111\rangle$	14.964	14.977			
$\|121\rangle$	15.220	15.251			

[a] CC: coupled channel.[68] D: matrix diagonalization. DMC: fixed-node DMC using [1]the appropriate IBC node, [2]adiabatic, and [3]accurate nodal functions. The $|jlJ\rangle$ labeling scheme is exact only for the isotropic binary complex.

TABLE 8: Ground and Excited-State Energies for the He−HBr Dimer in cm^{-1}[a]

dominant $\|jlJ\rangle$	CC	D	DMC[1]	DMC[2]	DMC[3]
$\|000\rangle$	−7.873	−7.881	−7.861 ± 0.076	−7.861 ± 0.076	−7.861 ± 0.076
$\|011\rangle$	−7.406	−7.414	−7.412 ± 0.034		
$\|101\rangle$	8.078	8.091	7.904 ± 0.081	8.561 ± 0.057	7.781 ± 0.131
$\|111\rangle$	10.463	10.455			
$\|121\rangle$	10.569	10.548			

[a] CC: coupled channel.[68] D: matrix diagonalization. DMC: fixed-node DMC using [1]the appropriate IBC node, [2]adiabatic and [3]accurate nodal functions. The $|jlJ\rangle$ labeling scheme is exact only for the isotropic binary complex.

and $\Psi_{\text{iso}}^{(b)} = \cos\theta_1$, where θ_1 and θ_2 are the space-fixed polar angles of the molecule and atom, respectively. Although it is legitimate to refer to the nodal function $\Psi_{\text{iso}}^{(b)}$ as the "free-rotor" node because this node is identical to that of the free molecule, analogous terminology for $\Psi_{\text{iso}}^{(a)}$ does not exist, because the orbital angular momentum of the atom has to be referred to some center, in this case, the com of the molecule. Thus, this node is neither a "free-atom" nor a "free-rotor" node. The IBC limit also provides a useful labeling scheme with which to correlate the levels of the anisotropic binary complex in the space-fixed frame.

Tables 6−8 show a selection of energy levels for the three dimers using coupled-channel, diagonalization and various DMC methods, as will be described.

3.1. Coupled-Channel Calculations for the Dimers. Coupled-channel calculations were performed for the three dimers using the BOUND program.[68] In this procedure, the potential was first expanded as in eq 9. The quality of the expansion was checked by (i) comparing contour plots of the accurate potential with those obtained from the expansion and (ii) examining the convergence of the computed eigenvalues as a function of λ (see eq 9). The radial strength functions were generated using a Gauss−Legendre quadrature. Coupled-channel (CC) results for several eigenvalues with $J = 0$ and $J = 1$ are shown in Tables 6−8 for the three molecules.

3.1.1. Matrix Diagonalization for the Dimers. In the fixed-node DMC calculations (to be described) for excited states, it is necessary to have good estimates of nodal surfaces. Previous work for the HCN−He complex has shown that the nodal functions of the IBC do not necessarily provide accurate estimates of the actual nodal geometries.[47,53] To gain insight into the distortion of the IBC nodal topologies due to the potential anisotropy, accurate eigenfunctions for the binary complex were computed using a basis set that is a product of $|\text{radial}\rangle \times |\text{angular}\rangle$ functions. The total wave function is expanded,

$$\Psi = R^{-1}\sum_a c_{jl}^{JM}\,\Phi_{j,l}^{JM}(\Omega_1, \Omega_2)\chi^{(n)}(R) \qquad (10)$$

where R is the intermolecular distance; $\Omega_1 = (\theta_1, \phi_1)$ is the spherical polar angular coordinates of the molecule, and $\Omega_2 = (\theta_2, \phi_2)$ is the spherical polar angular coordinates of the atom and $\{c_{jl}^{JM}\}$ are expansion coefficients. The radial basis functions, $\chi^{(n)}(R)$, where n is the radial quantum number, were chosen to be harmonic oscillator eigenfunctions. The angular basis functions $\Phi_{j,l}^{J,M}(\Omega_1, \Omega_2)$ are defined as follows

$$\Phi_{j,l}^{J,M}(\Omega_1, \Omega_2) = \sum_{m_j,m_l} (-1)^{j-l+M}\sqrt{(2J+1)} \times \begin{pmatrix} j & l & J \\ m_j & m_l & -M \end{pmatrix} Y_j^{m_j}(\Omega_1) Y_l^{m_l}(\Omega_2) \qquad (11)$$

where $\begin{pmatrix} \cdots \end{pmatrix}$ is a Wigner 3-j symbol and $Y_j^{m_j}(\Omega_1)$ and $Y_l^{m_l}(\Omega_2)$ are spherical harmonics. Using the expansion in eq 9, the matrix elements of the potential can be expressed in closed form in terms of Percival−Seaton coefficients.[67] The size of the basis is determined by the maximum size of $j = j_{\max}$ for a given J. The matrix diagonalization results in Tables 6−8 compare favorably with coupled channel and literature values for states with $J = 0, 1$.

4. Rigid-Body Diffusion Monte Carlo Calculations

The DMC calculations were performed using the rigid-body diffusion Monte Carlo (RBDMC) method originally developed by Buch[70] and later extended to compute excited states using importance sampling.[38,71] This procedure reduces the number of degrees of freedom and allows larger diffusive time steps to be made. The RBDMC approximation is especially suitable for very weakly bound complexes because of the large difference in the strengths of the intramolecular and intermolecular forces and, therefore, in the time scales of the various motions. The

basic idea in RBDMC is to recognize that for sufficiently small rotations, the rotational energy propagator is analogous to the translational kinetic energy propagator with a diffusion constant $D_R = 1/2I$ where I is the moment of inertia of the molecule. This procedure takes advantage of the fact that components of angular momentum commute for sufficiently small rotations. In the current application, all translations and rotations are made in a rotor-fixed frame, that is, rotational moves are done around the set of principal axes of the HX com, which rotates along with the rigid HX molecule.

In RBDMC, excited rotational states are computed using the fixed-node method:[72,73] in essence, this involves "killing" walkers that cross nodal surfaces. In the simulations, importance sampling was used, as is now described.

4.1. Importance Sampling. In importance sampling, a trial wave function, Ψ_T, is introduced to guide the diffusion process. This improves the efficiency of the DMC method and increases the precision of the computed energies.[72] For larger He clusters, unphysical dissociation may occur unless importance sampling is used. Use of a guiding trial wave function leads to a diffusion-like equation for the mixed function $f(\mathbf{R}, \mathbf{r}_i) = \Psi(\mathbf{R}, \mathbf{r}_i)\Psi_T(\mathbf{R}, \mathbf{r}_i)$, where $\mathbf{R}$ and $\mathbf{r}_i$ are the molecular and He atom coordinates respectively. Additional drift terms (quantum forces) that guide the walkers to regions of high probability density[74] are introduced into the diffusive process. In this work, trial wave functions were chosen to have the form

$$\psi_T = \left\{\prod_{i=1}^{N} f(R_i) \prod_{i\neq j}^{N} \Xi(r_{ij})\right\} \mathrm{Y}(\Omega, \theta_i, \phi_i) \qquad (12)$$

where R_i is the radial distance from the molecular com to helium atom i and r_{ij} is the distance between helium atoms i and j. As in previous work,[38,47,53] the radial functions were of the following form.

$$f(R) = b \exp\left(-\frac{c}{R^5} - aR\right) \qquad (13)$$

The parameters a, b, and c were obtained by fitting the function $f(R)$ to (i) accurate binary wave functions obtained from diagonalization or (ii) adiabatic radial functions. The two approaches provided similar results. For ground-state calculations, the angular function $\mathrm{Y}(\Omega_1, \Omega_2)$ was set to unity, whereas for excited states, this function contains the nodal topology. However, for some nodal functions used in which the full set of space-fixed angles appear, it was found preferable simply to kill walkers that crossed the node using a recrossing correction. This was done to avoid the computation of derivatives of the nodal part of the wave function, which has to be done numerically. We found that using numerical derivatives introduced errors into the diffusion process as well as slowed it down considerably. Pilot calculations demonstrate that killing walkers at the nodes without building the nodal structure explicitly into the trial wave function provides excellent results. The He−He part of the trial wave function, $\Xi(r_{ij})$, was the same as that used in previous studies.[38,53]

5. Ground State Properties

We performed systematic studies of ground states properties, that is, energy levels and radial and angular distributions, for all three HX complexes with various numbers of helium atoms, by means of unbiased RBDMC.

5.1. The Three Dimers. The most obvious difference among the three dimers, He−HF, He−HCl, and He−HBr, is in the ordering of the potential minima. Table 5 indicates that for He−HF, the configuration He−HF has a deeper well than does He−FH; for He−HCl and He−HBr, this ordering is inverted. Figures 3−5 compare the He density computed for the three complexes assuming that the gas-phase rotational constant $B_0 = 0$ with those obtained using the physical values. In the case of no rotation ($B_0 = 0$), the density for HF and HCl is primarily concentrated at the H atom end of the HX molecule, whereas for HBr, the opposite is the case. The finding that the He−HCl configuration is favored over the He−ClH configuration agrees with the results of Murdachaew et al.[57] obtained using a different PES. This was attributed to the greater volume of the shallower well in the He−HCl configuration; that is, despite the well's being shallower, the volume of phase space is greater at the H end of the molecule. It should also be noted that the ground state of the HCl−He dimer actually lies *above* the saddle point of the PES.

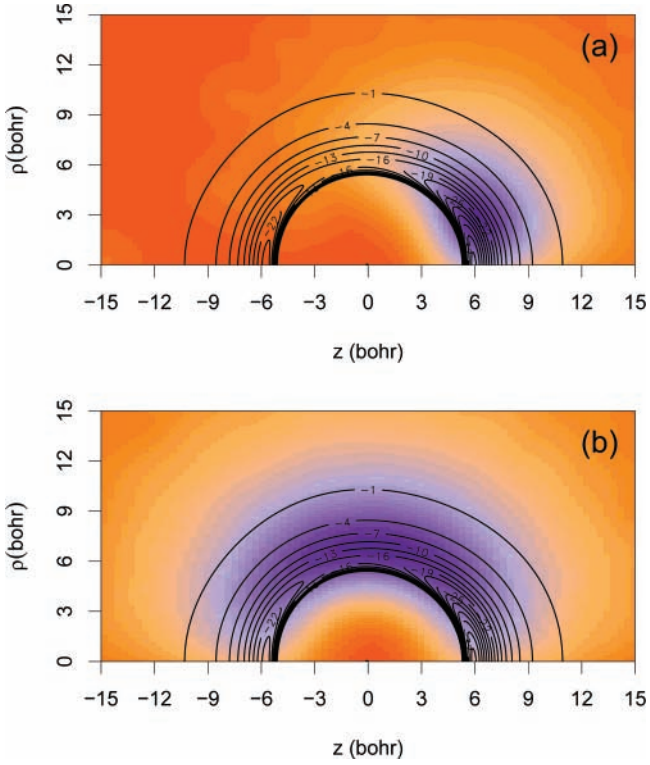

Figure 3. Density distributions of DMC walkers superimposed on the PES of He−HF in cylindrical coordinates, ρ, z, where $\rho = \sqrt{x^2+y^2}$. (a) $B = 0$ and in (b) $B = B_0$, where B_0 is the physical (gas-phase) value of the rotational constant. The H atom of the HF molecule lies along the positive z-axis. In panel (a), the DMC walkers gather around the potential minimum, whereas in panel (b), walkers spread out more as a result of rotation of the molecule, indicative of larger decoupling between the molecule and helium. The color scale shows the density of walkers and goes from orange (low) to blue (high) color. Contours are of the PES in cm^{-1}.

5.2. Radial and Angular Distributions. Figures 6−8 show the radial probability functions as a function of number of He atoms. The corresponding angular probability functions are shown in Figures 9−11. These plots were obtained by projection of the He density from converged unbiased RBDMC calculations into a frame in which the molecule is aligned along the space-fixed z-axis with the H atom along the positive z-axis. The radial and angular distributions were computed using the ground-state probability density, $|\langle x|100\rangle|^2$.

For a given He−HX complex, all radial distribution functions peak around the same R value. This finding suggests that up to $N = 15$, He atoms fill up only the first solvation shell around the molecule, and the second solvation shell has not yet begun.

It is apparent from Figures 9−11 that for $N = 1$, though delocalized, the density switches primarily from the H end of

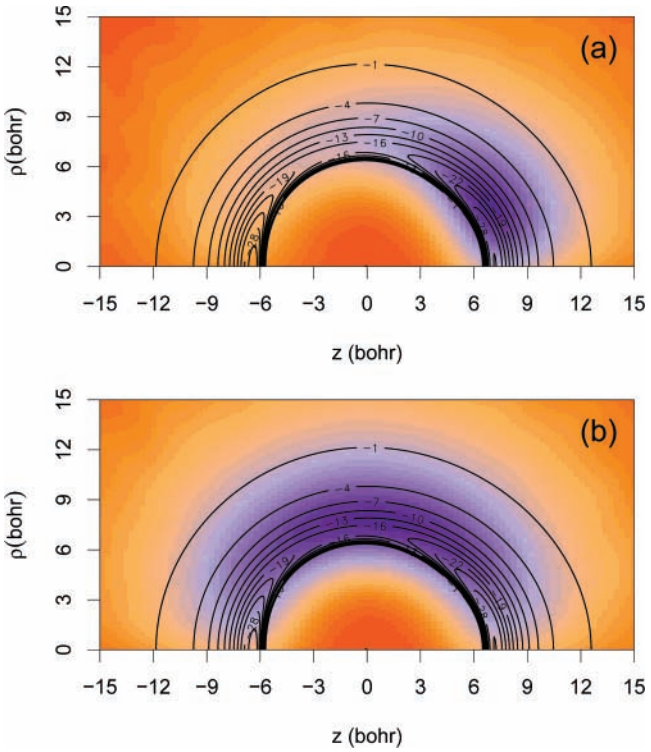

Figure 4. Same as Figure 3, but for He−HCl.

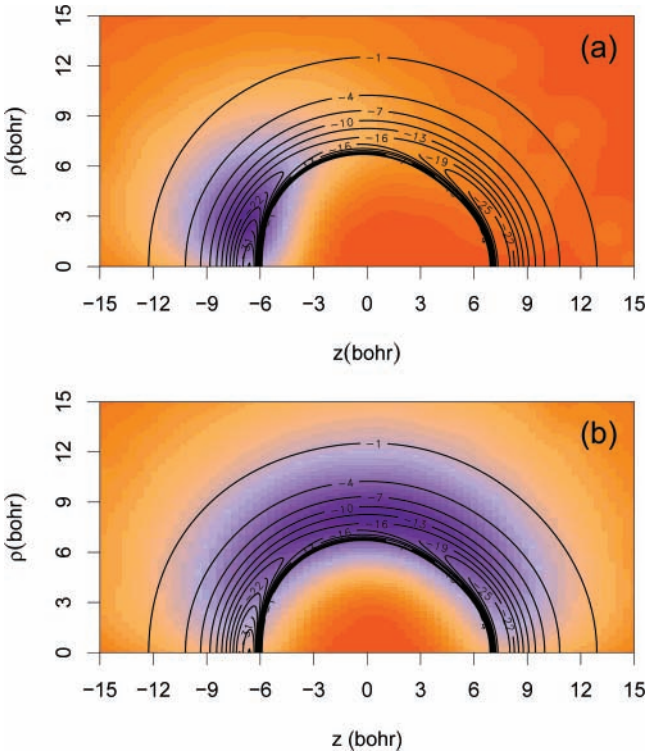

Figure 5. Same as Figure 3, but for He−HBr.

the molecule in HF and HCl to the halogen end in HBr. For larger numbers of He atoms, the majority of the density in all cases is concentrated in a broad donut shape around the waist of the molecule. The effect of the relatively large value of B_0 for all three molecules is clearly reflected in the significant delocalization of the He density, as compared to the case that $B = 0$. Given the large B_0 values, one would expect a rather modest decrease in the effective rotational constant for these molecules in a helium-4 nanodroplet. In fact, for HF, $B_{\text{eff}} \sim 98\%$.[16,75] Simply on the basis of the size of B_0, one would expect somewhat larger percentage reductions for HCl and HBr. This is the subject of the next section.

6. Excited States

Excited states were computed using fixed-node DMC and, in particular, the ANDMC method proposed by Mikosz et al.[47] In this approach, improved (as compared to the IBC) estimates of nodal surfaces are obtained by making an adiabatic separation of radial and angular motions. The excited states computed using different fixed nodes in the DMC procedure are collected together in Tables 6−8. The differences between the results can be entirely attributed to differences in the quality of the nodal topology used. Even when an accurate nodal surface is employed, there is some deviation from the accurate result; this is related to the fact that, even with a numerically exact node to hand, approximations are nevertheless present in the fixed-node procedure. For example, recrossing corrections can be used to improve accuracy. However, this is technically difficult to do in the case that the nodal topology is complicated, as in the current application.

In the current study, the computations are done for clusters containing up to $N = 20$ He atoms. In principle, much larger clusters could be studied using Monte Carlo methods. However, as the number of particles increases, the error bars on the energies also increase. Beyond $N = 20$, it becomes very difficult to converge the effective rotational constant, which is obtained from calculating the difference between the ground and excited rotational states. However, because quantum solvation (i.e., saturation of B_{eff}) may occur relatively rapidly as a function of N,[40,51,52] although larger clusters may exhibit interesting features,[43] we expect that the essential angular momentum coupling and decoupling mechanism will be captured in these simulations.

6.1. Nodal Surfaces of the Dimers, He−HX. The topologies of the wave functions can best be understood by considering the expansion of the PES in Legendre polynomials in eq 9. Plots of the first four dominant $v_\lambda(R)$ functions are shown in Figure 2. The P_1 term mixes zero-order basis states with $\Delta j, \Delta l = \pm 1$. For the three dimer complexes, the free-rotor state $|101\rangle$ is coupled most strongly to $|011\rangle$ by the P_1 anisotropy, whereas the P_2 anisotropy leads to admixtures containing primarily $|121\rangle$.[67] Unlike in the case of He−HCN,[47] the dominant potential anisotropy for the three complexes arises from the P_2 term in eq 9. Furthermore, as one moves through the series HeHF−HeHCl−HeHBr, the minimum in the corresponding strength function, $v_2(R)$, moves closer to the minimum in $v_0(R)$ while its well depth becomes shallower in comparison to v_0.

Figure 12 is a representation of the probability density of the space-fixed wave function, $|\langle x|101\rangle|^2$ for the HF−He dimer obtained from diagonalization. The nodal surface is clearly apparent and corresponds roughly to the plane $\theta_1 \approx \pi/2$. This can be traced to the dominance of the P_2 radial strength function. The plots are similar for the HCl−He and HBr−He dimers. In these three cases, and again unlike for HCN, the "free-rotor" nodal surface provides a reasonable approximation to the actual dimer node. Note that the "free-rotor" approximation improves as the one goes from HF to HCl to HBr. This is apparent upon comparing the rotational energies obtained using the free-rotor nodal function in DMC with accurate results in Tables 6−8. As the mass of the system increases, the wave function becomes somewhat more localized, which tends to "clean up" the node. In addition, the system is becoming somewhat more isotropic, that is, the nonspherical radial strength functions contribute less. For more than a single He atom, the nodal surfaces can be estimated using the adiabatic procedure now described.

6.2. Adiabatic Nodal Functions. Holmgren et al.[48] developed an adiabatic, that is, Born−Oppenheimer-like, angular−radial

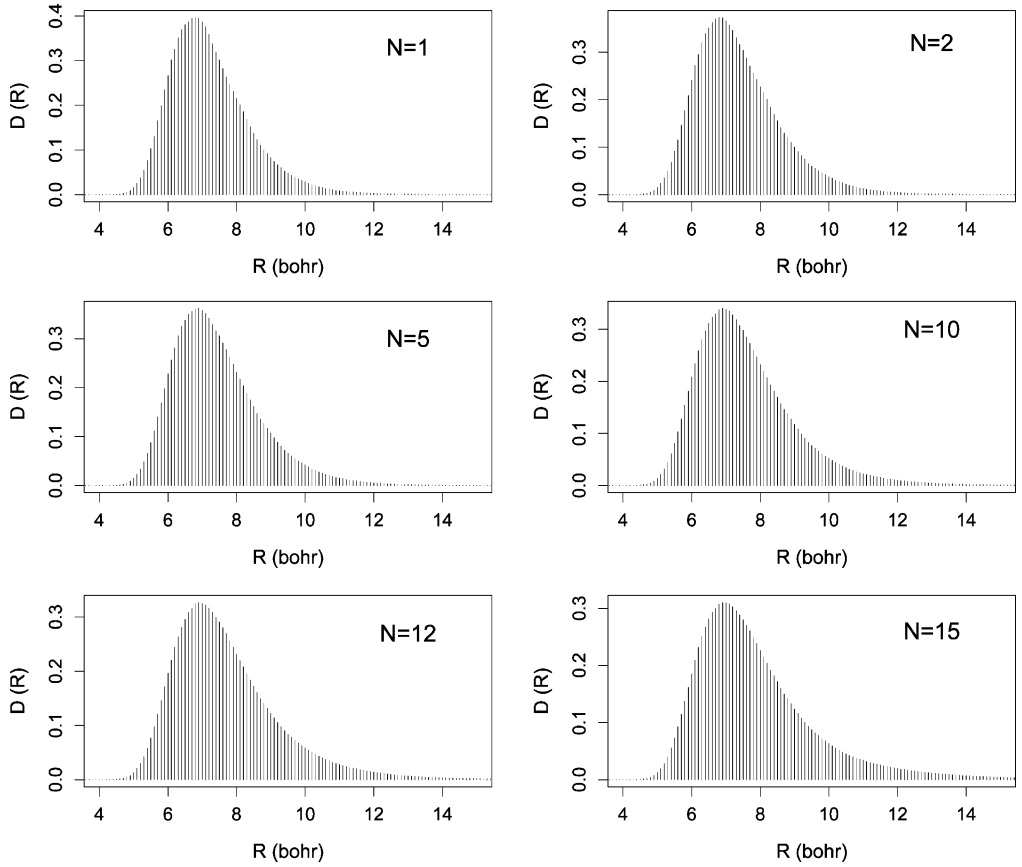

Figure 6. Radial distribution functions, $D(R) = 4\pi R^2 \mathscr{R}(R)^2$ for HF−He_N clusters, where R is the distance between the com of the molecule and the He atom, $\mathscr{R}(R)$ is the radial part of the wave function, and N is the number of He atoms solvating the diatom. All probabilities are normalized to unity.

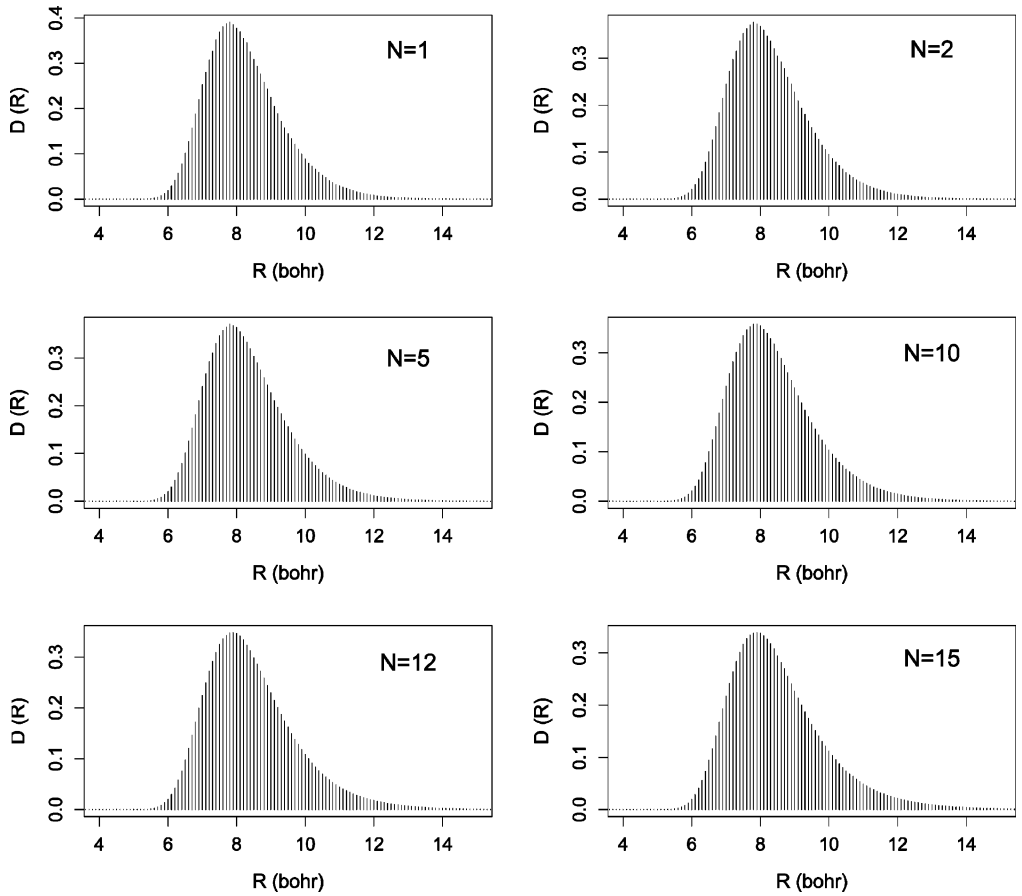

Figure 7. Same as Figure 6, but for He−HCl.

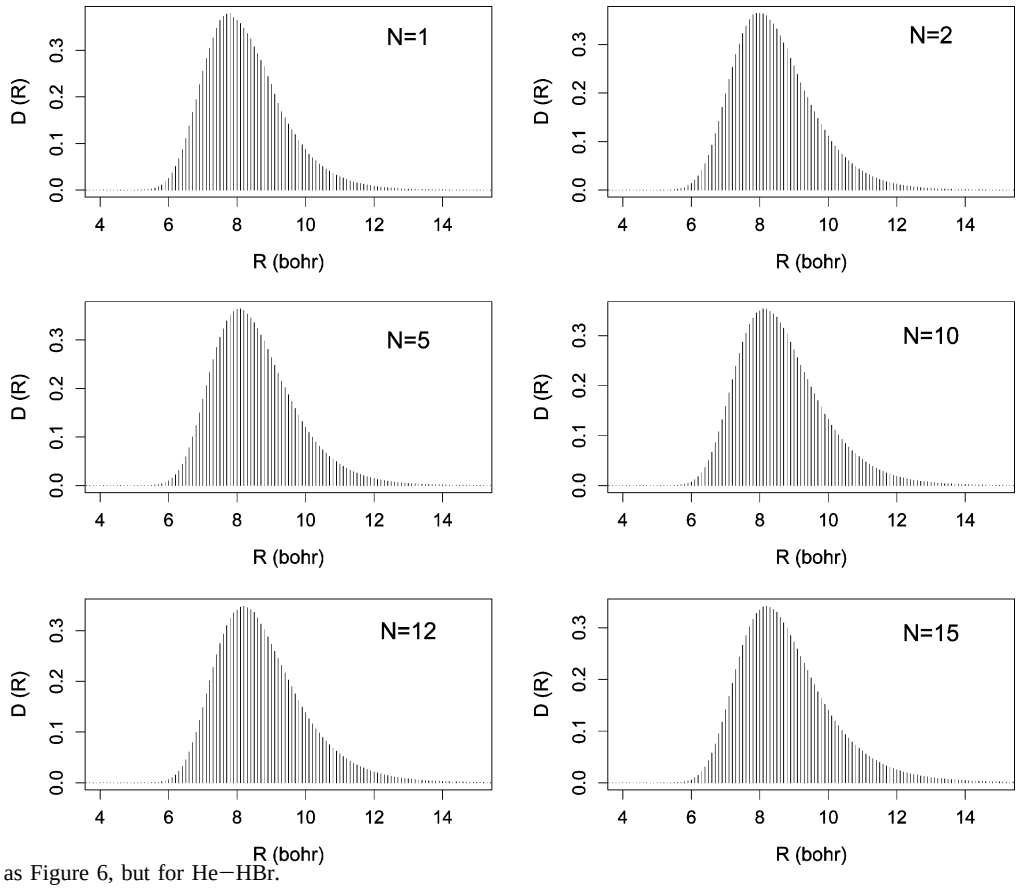

Figure 8. Same as Figure 6, but for He−HBr.

separation (BOARS) in the molecule fixed frame for van der Waals atom−molecule dimer complexes. In BOARS, the radial degree of freedom is frozen at $R = R_0$, and the angular part of the resulting Schrödinger equation is then solved; this is repeated for different values of R_0, which generates families of adiabatic radial potentials. The adiabatic potentials are then used to solve for the radial wave functions. Although the BOARS approach has generally been superseded for atom−molecule (dimer) van der Waals complexes, it nevertheless can be adapted to provide a convenient and accurate way of generating good estimates of nodal surfaces for small molecule−helium clusters.[47] The method is also computationally quite efficient because the angular matrix elements can be computed analytically or semianalytically.[67,76]

Adiabatic nodal functions are computed by making the following assumptions: (i) He−He interactions are ignored (for ground states with $N = 10$, for example, these contribute <5% to the energy); (ii) fix $R = R_0$; (iii) pin the molecular com in place; (iv) for more than a single He atom, the adiabatic separation is done in the space-fixed frame.

The resulting Hamiltonian is the following

$$H_{\mathrm{rot}} = B_0\mathbf{j}^2 + \sum_{i=1}^{N} \kappa \mathbf{l}_i^2 + \sum_{i=1}^{N} V(R_0, \theta_{iI}) \qquad (14)$$

where $\kappa = 1/2mR_0^2$. Diagonalizing H_{rot} at fixed J and N thus produces estimates for the nodes. The value of R_0 is chosen to be the minimum of the appropriate adiabatic radial potential. Alternatively, R can be treated as a free parameter for the dimer and varied to obtain the best agreement with accurate results. This value is then used for clusters containing more than one He atom.

e;1.0qDiagonalization involves the coupling of $N + 1$ angular momenta. For example, consider the case that four (rotor + three He atoms) angular momenta are involved, that is, $\mathbf{j}$, $\mathbf{l_1}$, $\mathbf{l_2}$, $\mathbf{l_3}$ where the quantum numbers j, m_j refer to the rotor and l_i, m_i, $i = 1, 2, 3$ to the He atoms. Because the He atoms are equivalent, the following angular momentum coupling scheme is used. Form the intermediate angular momenta, $\mathbf{l_{12}} = \mathbf{l_1} + \mathbf{l_2}$, $\mathbf{l_{123}} = \mathbf{l_{12}} + \mathbf{l_3}$, and then form the total angular momentum, $\mathbf{J} = \mathbf{j} + \mathbf{l_{123}}$. The basis functions can then be expressed in terms of generalized Clebsch−Gordan coefficients; for example, for $N = 3$, the basis functions may be written[49,77−79]

$$\psi^{JM}_{jl_1l_2l_3l_{12}l_{123}} = \sum_{m_j,m_1,m_2,m_3}^{N} C(l_1m_1 \ldots l_{123}m_{123}jm_jJM) \times Y_j^{m_j}(\Omega_j)Y_{l_1}^{m_1}(\Omega_1)Y_{l_2}^{m_2}(\Omega_2)Y_{l_3}^{m_3}(\Omega_3) \qquad (15)$$

where $C(l_1m_1 \ldots l_{123}m_{123}jm_jJM)$ is a generalized Clebsch−Gordan coefficient[77] and $\Omega_{j,i}$ refer to the space-fixed coordinates of the several rotors. Explicitly,

$$C(jm_jl_1m_1l_2m_2l_3m_3l_{12}m_{12}l_{123}m_{123}JM) = \sum_{m_{12},m_{123}} (-1)^{l_{12}-m_{12}+l_{123}-m_{123}} \times \begin{pmatrix} l_1 & l_2 & l_{12} \\ m_1 & m_2 & -m_{12} \end{pmatrix} \times \begin{pmatrix} l_3 & l_{12} & l_{123} \\ m_3 & m_{12} & -m_{123} \end{pmatrix} \times \begin{pmatrix} j & l_{123} & J \\ m_j & m_{123} & -M \end{pmatrix} \qquad (16)$$

The matrix elements of H_{rot} are computed using the Wigner−Eckhardt theorem.[67,77,79]

In previous work on HCN complexes, the value of R used was chosen to correspond to the minimum of the adiabatic radial potential.[47] Inspection of the PESs in Figure 1 indicates that as one moves from HF to HCl to HBr, the two potential minima move to different R values relative to each other. This radial distortion suggests that use of a single R value to define the

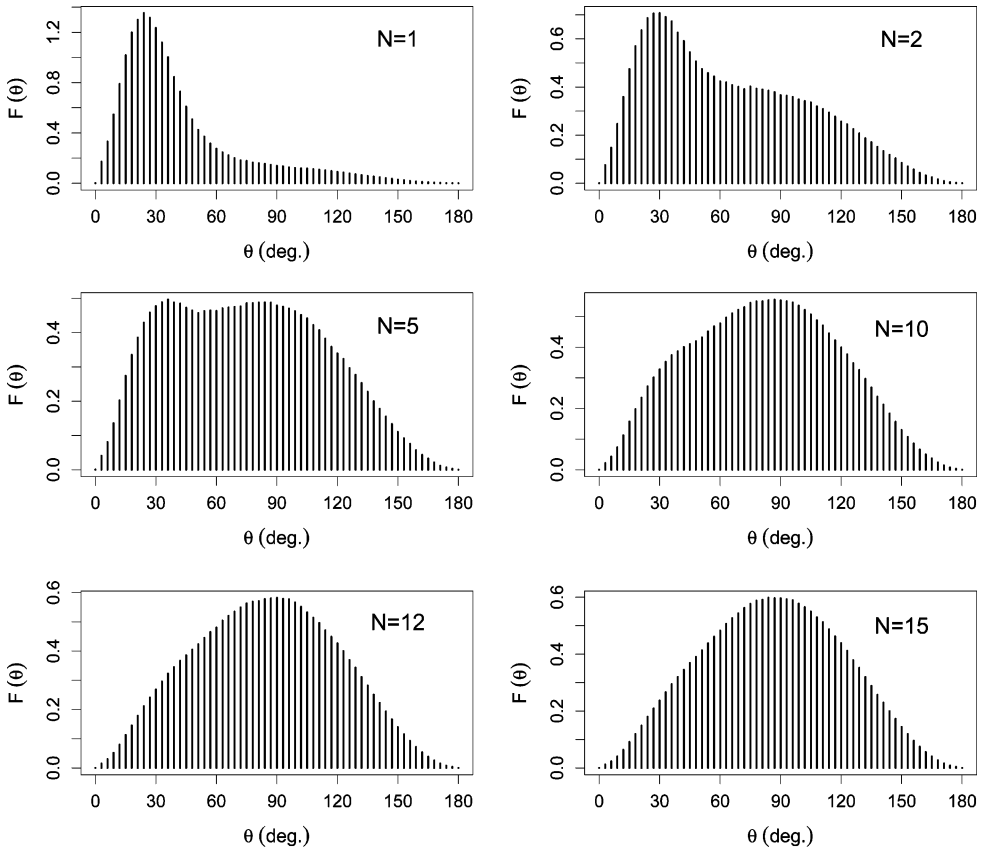

Figure 9. Angular distribution functions, $F(\theta) = 2\pi Y(\theta)^2 \sin\theta$ for HF−He$_N$ clusters, where θ is the angle between the molecular axis and the vector **R** connecting the molecule com and the He atom, and $Y(\theta)$ is the θ-dependent part of the angular part of the wave function. Here, 0° corresponds to the H end of the molecule. All probabilities are normalized to unity.

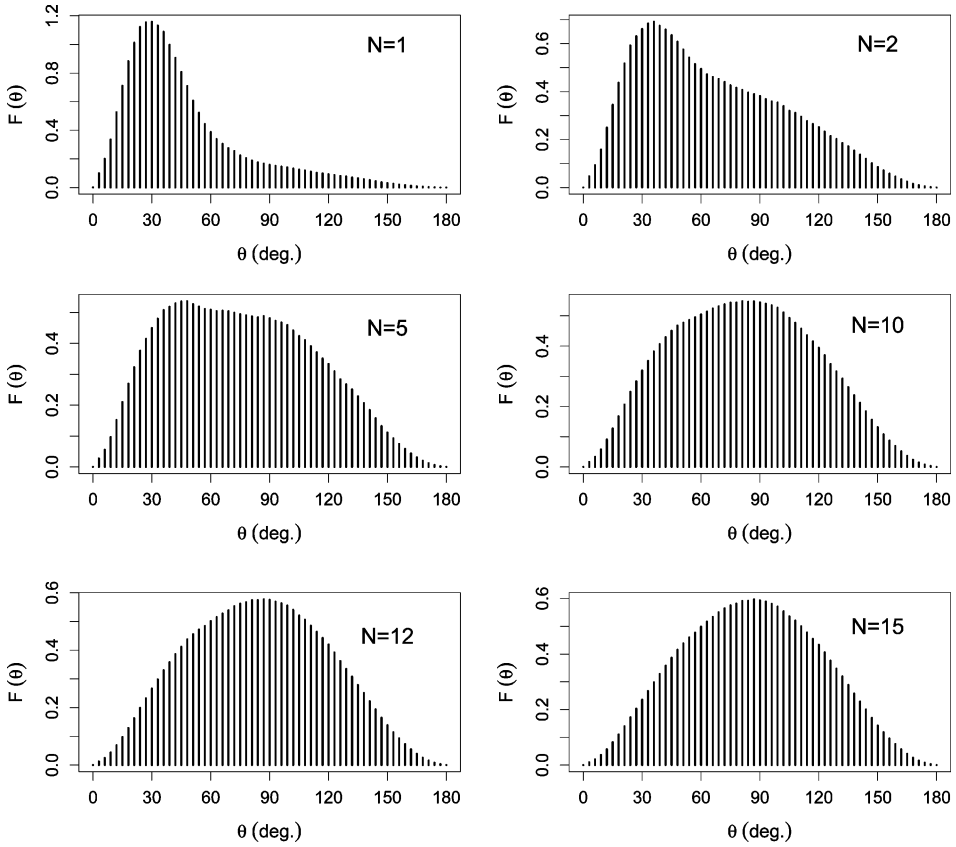

Figure 10. Same as Figure 9, but for He−HCl.

node might be a less good approximation in HF than HBr. In fact, for the nominal $|101\rangle$ state, both the free-rotor ($\cos\theta_1$) and "single R" adiabatic nodes provide reasonable agreement with accurate results. However, some improvement can be

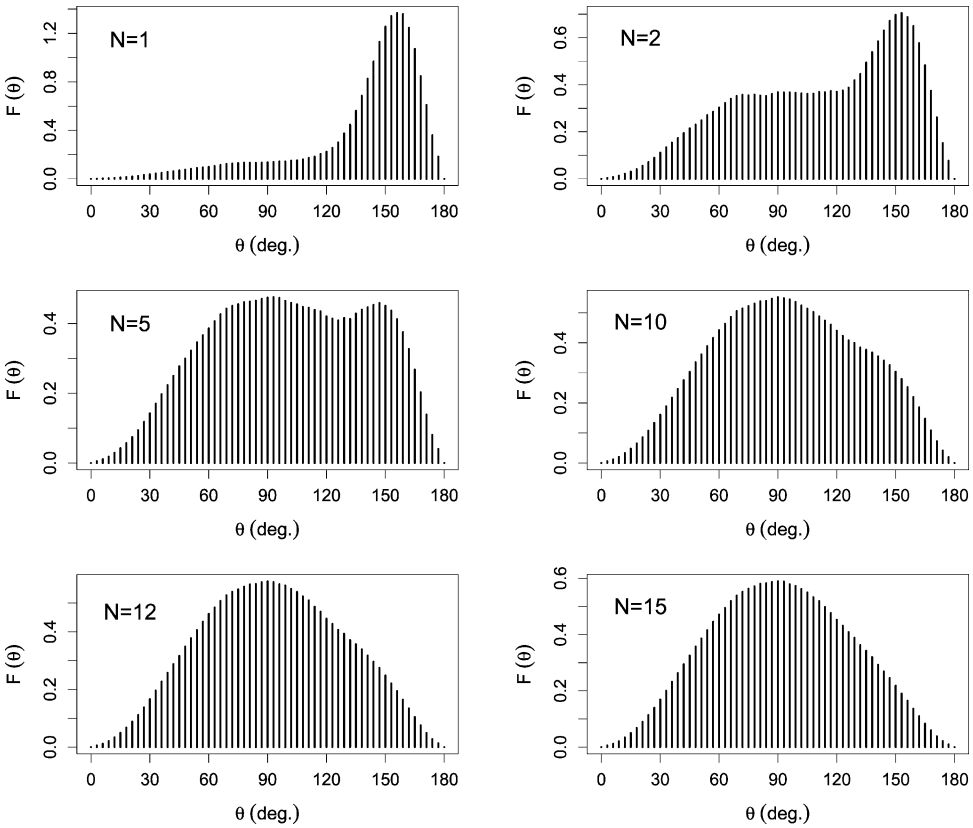

Figure 11. Same as Figure 9, but for He−HBr.

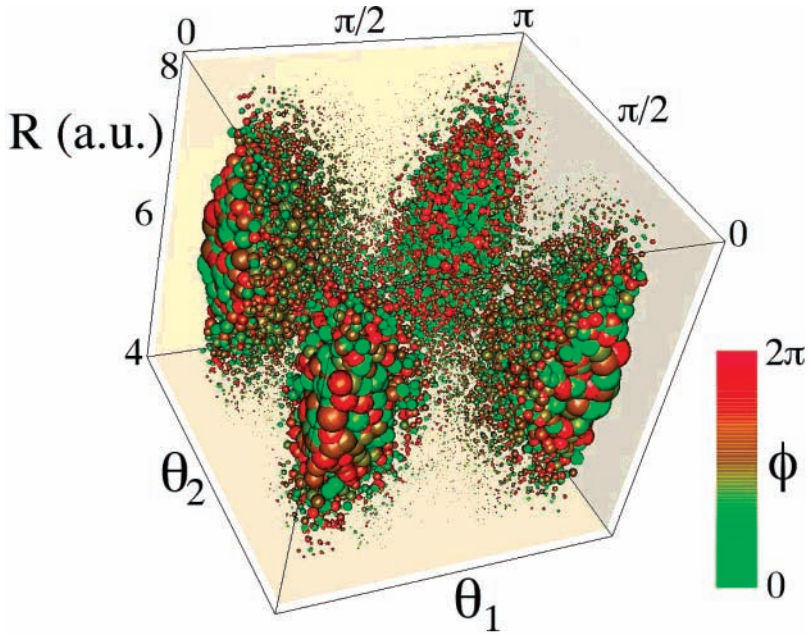

Figure 12. Three-dimensional scatter plot of the probability density of the $|101\rangle$ space-fixed state obtained from diagonalization for the He−HF dimer, that is, $|\langle x|101\rangle|^2$. The angles θ_1 and θ_2 are the space-fixed polar angles of the HF molecule and the He atom, respectively, in radians; $\phi = \phi_1 - \phi_2$ is the relative azimuthal angle; R is the distance, in atomic units (a.u., i.e., bohrs), between the He atom and the HF center of mass. To generate the plot, 20 000 points were chosen randomly in (θ_1, θ_2, ϕ, R) space with $4 < R < 10$ bohr. Points in (R, θ_1, θ_2) space are represented by spheres whose size is proportional to $|\langle x|101\rangle|^2$. Each sphere is colored according to its value of ϕ as indicated in the color scale bar. The equilibrium value of R is ~ 6 bohr. The plane $\theta_2 = \pi/2$ does not correspond to a nodal surface because the wave function does not change sign as one crosses this surface. The nodal surface is roughly the same as the "free-rotor" node; that is, the plane $\theta_1 = \pi/2$.

achieved by using the following procedure to generate adiabatic nodal surfaces:

(1) Generate adiabatic wave functions on a grid of R values.

(2) The adiabatic wave function is then represented as

$$\psi(\Omega_1, \Omega_2; R) = \sum c(R)\psi^{JM}_{jl_1l_2l_3l_{12}l_{123}}(\Omega_1, \Omega_2; R) \quad (17)$$

(3) Finally, the expansion coefficients, $c(R)$, are fitted to an analytical form. In practice, Morse potential forms provide an

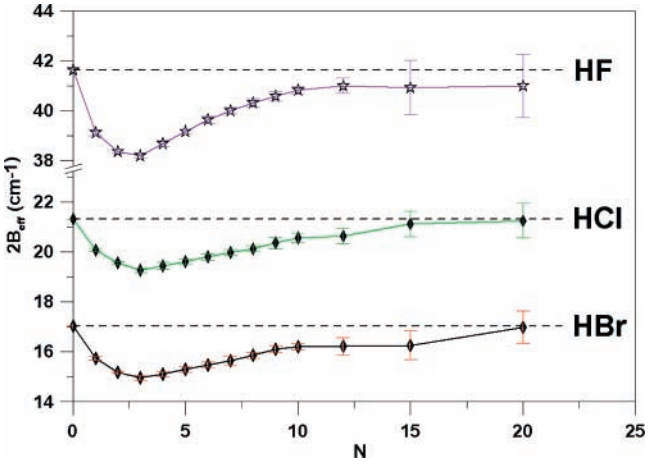

Figure 13. Values of the rotational energy of the states that evolve from $|101\rangle$ for the three HX molecules as function of the number of He atoms, N. Energies are expressed in terms of $2B_{\text{eff}}$, where B_{eff} is the effective rotational constant and is defined as $B_{\text{eff}} = (E^{(101)} - E^{(000)})/2$. The horizontal dashed lines show the value of $2B_0$; that is, the gas-phase value of the free molecule.

accurate fit over the range of interest. The function ψ in eq 17 is then used to define the nodal function in the trial wave function.

The result of using adiabatic nodes is shown for the three dimer complexes in Tables 6−8. For more than a single He atom, adiabatic nodes provide results that are very similar to when the free-rotor node is employed. Figure 13 shows values of the rotational energy of the states that evolve from $|101\rangle$ for the three HX molecules as a function of the number of He atoms, N. Energies are expressed in terms of "$2B_{\text{eff}}$". Note that by $N = 20$ for both HCl and HBr, B_{eff} for HF is similar to the experimental nanodroplet limit, albeit for the $v = 1$ state of HF. The results shown in Figure 13 were obtained using a free-rotor nodal function. In this case, adiabatic nodal functions give very similar results, especially for $N \geq 2$. This contrasts sharply with the situation for HCN in which the free-rotor node provides poor agreement with accurate results for small number of He atoms.[47] This result can be understood in terms of the contributions of the different anisotropic components of the PES: He−HCN and He−CO are "P_1"-type dimers, whereas the He−HX complexes are dominantly P_2-type (see Figure 2).

6.3. Nodal Decoupling. The transition from the relatively strong coupling in the dimer to the solvated molecule can be understood in terms of angular momentum coupling between the molecule and the He atoms. Consider first the dimer, that is, $N = 1$. For $J = 1$, the dominant states are $|011\rangle$ and $|101\rangle$. The P_1 term mixes zero-order basis states with Δj, $\Delta l = \pm 1$ and to lowest order, the resulting states have the form $|a\rangle = c_1|011\rangle + c_2|101\rangle$, $|b\rangle = -c_2|011\rangle + c_1|101\rangle$ with $|c_1|^2 + |c_2|^2 = 1$. By contrast, the P_2 anisotropy leads mainly to admixturesof $|101\rangle$ and $|121\rangle$. The corresponding wave functions can be written explicitly as follows:

$$\psi_{101} = \frac{\sqrt{3}\cos\theta_1}{4\pi} \tag{18}$$

$$\psi_{121} = -\frac{1}{4\pi}\sqrt{\frac{3}{2}}(\cos\theta_1(3\cos^2\theta_2 - 1) + 3\cos\phi\cos\theta_2\sin\theta_1\sin\theta_2)$$

where $\phi = \phi_1 - \phi_2$ and the subscript "1" (2) refers to the angular coordinates of the molecule (atom). For N He atoms, the $|121\rangle$ state is replaced by a symmetric linear combination of states having He orbital angular momenta permuted over the N He atoms; for example, $|jl_1l_2l_3l_{12}JM\rangle = |120020JM\rangle$, $|102020JM\rangle$, etc. Denoting these normalized "solvent" states by $|s\rangle/\sqrt{N}$ and "molecule" states of the form $|10...00...0JM\rangle$ by $|j\rangle$, the eigenvector mixtures to lowest order are the same as for $N = 1$. For example,

$$|\alpha\rangle \approx \frac{c_1}{\sqrt{N}}|s\rangle + c_2|j\rangle \tag{19}$$

The factor of $1/\sqrt{N}$ diminishes the contribution of each individual He atom as N increases. Furthermore, as N increases, the trigonometric terms will approach their average values; that is, the free-rotor "cos θ_1" term will emerge. In fact, as Figure 12 shows, the free-rotor node is quite good, even for $N = 1$.

7. Conclusions

Ground- and excited-state properties were computed for the HX(^{4}He)$_N$, complexes with $N = 1 - 20$ and $X =$ F, Cl, Br. The calculations used pairwise intermolecular potentials specifically computed for the He−HX interactions and fitted to similar functional forms. Intermolecular energies and ground-state He radial and angular probability density distributions were computed. Excited states were calculated using a fixed-node DMC procedure. Molecule−solvent angular momentum coupling was studied as a function of cluster size and potential anisotropy. The calculations suggest that the observed decrease in the gas-phase rotational constants for HCl and HBr in a helium-4 nanodroplet will be smaller than for HF, despite HF's having a considerably larger rotational constant than the other two molecules.

Generally, these results can be explained in terms of the interplay between the various anisotropies of the potential energy surfaces shown in Figure 2 for the HF−He, HCl−He, and HBr−He potentials. In contrast to HCN[47] and CO, for which the P_1 and P_2 anisotropies compete, for quantum solvated hydrogen halides, the P_2 anisotropy dominates. The solvation behavior of the three molecules can be traced to how the potential anisotropies couple angular momentum states between the molecule and the bosonic helium-4 atoms. Although HF has a rotational constant that is almost double that of HCl, the somewhat larger anisotropy of the PES leads to a small asymptotic decrease in the effective rotational constant, whereas HCl and HBr approach their gas-phase values in the nanodroplet limit.

Acknowledgment. This paper is dedicated to Professor Giacinto Scoles on the occasion of his 72nd birthday and in recognition of his outstanding contributions to science in general and physical chemistry in particular. This work has been supported in part by the National Science Foundation (U.S.A.) and in part by NANOQUANT RTN, Contract no. MRTN-CT-2003-506842, and by the Ministerio de Educación y Ciencia (Spain) and FEDER (CTQ2005-01076 project).

References and Notes

(1) Wilks, J.; Betts, D. S. *An Introduction to Liquid Helium*; Clarendon Press: Oxford, U.K., 1987.
(2) Tilley, D. R.; Tilley, J. *Superfluidity and Superconductivity*; Institute of Physics: Bristol, U.K., 1990.
(3) Leggett, A. J. *Acta Fenn.* **1973**, *8*, 125−170.
(4) Northby, J. A. *J. Chem. Phys.* **2001**, *115*, 10065−10077.
(5) Ceperley, D. M. *Rev. Mod. Phys.* **1995**, *67*, 279−355.

(6) Toennies, J. P.; Vilesov, A. F. *Angew. Chem., Int. Ed.* **2004**, *43*, 2622−2648.
(7) Kim, E.; Chan, M. H. W. *Science* **2004**, *305*, 1941−1944.
(8) Leggett, A. J. *Science* **2004**, *305*, 1921−1922.
(9) Dash, J. G.; Wettlaufer, J. S. *Phys. Rev. Lett.* **2005**, *94*, 235301-1−235301-4.
(10) Day, J.; Beamish, J. *Phys. Rev. Lett.* **2006**, *96*, 105304-1−105304-4.
(11) Grisenti, R. E.; Schöllkopf, W.; Toennies, J. P.; Hegerfeldt, G. C.; Köhler, T.; Stoll, M. *Phys. Rev. Lett.* **2000**, *85*, 2284−2287.
(12) Efimov, V. N. *Phys. Lett. B* **1970**, *33*, 563−564.
(13) Kraemer, T.; Mark, M.; Waldburger, P.; Danzl, J. G.; Chin, C.; Engeser, B.; Lange, A. D.; Pilch, K.; Jaakkola, A.; Nägerl, H.-C.; Grimm, R. *Nature* **2006**, *440*, 315−318.
(14) Barranco, M.; Guardiola, R.; Hernández, S.; Mayol, R.; Navarro, J.; Pi, M. *J. Low Temp. Phys.* **2006**, *142*, 1−81.
(15) Pandharipande, V. R.; Pieper, S. C.; Wiringa, R. B. *Phys. Rev. B: Condens. Matter Mater. Phys.* **1986**, *34*, 4571−4582.
(16) Callegari, C.; Lehmann, K. K.; Schmied, R.; Scoles, G. *J. Chem. Phys.* **2001**, *115*, 10090−10110.
(17) Wyatt, A. F. G., Lauter, H. G., Eds. *Excitations in two and three dimensional quantum fluids*; Plenum: New York, 1991.
(18) Nauta, K.; Miller, R. E. *Science* **1999**, *283*, 1895−1897.
(19) Scoles, G.; Lehmann, K. K. *Science* **2000**, *287*, 2429−2430.
(20) Lehmann, K. K.; Scoles, G. *Science* **1998**, *279*, 2065−2066.
(21) Hartmann, M.; Miller, R. E.; Toennies, J. P.; Vilesov, A. F. *Science* **1996**, *272*, 1631−1634.
(22) Nauta, K.; Miller, R. E. *Science* **2000**, *287*, 293−295.
(23) Dong, F.; Miller, R. E. *Science* **2002**, *298*, 1227−1230.
(24) Merritt, J. M.; Rudić, S.; Miller, R. E. *J. Chem. Phys.* **2006**, *124*, 084301−1 − 084301−12.
(25) Grebenev, S.; Toennies, J. P.; Vilesov, A. F. *Science* **1998**, *279*, 2083−2086.
(26) Grebenev, S.; Sartakov, B.; Toennies, J. P.; Vilesov, A. F. *Science* **2000**, *289*, 1532−1535.
(27) Whaley, K. B. *Int. Rev. Phys. Chem.* **1994**, 41−84.
(28) Whaley, K. B. *Adv. Mol. Vibr. Coll. Dyn.* **1998**, *III*, 397−451.
(29) Toennies, J. P.; Vilesov, A. F. *Annu. Rev. Phys. Chem.* **1998**, *49*, 1−41.
(30) Stienkemeier, F.; Lehmann, K. K. *J. Phys. B: At., Mol. Opt. Phys.* **2006**, *39*, R127−R166.
(31) Scheidemann, A.; Schilling, B.; Toennies, J. P. *Physica B* **1990**, *165*, 135−136.
(32) Lewerenz, M.; Schilling, B.; Toennies, J. P. *J. Chem. Phys.* **1995**, *102*, 8191−8207.
(33) Nauta, K.; Moore, D. T.; Stiles, P. L.; Miller, R. E. *Science* **2001**, *292*, 481−484.
(34) Xu, Y.; Blinov, N.; Jäger, W.; Roy, P.-N. *J. Chem. Phys.* **2006**, *124*, 081101−1 − 081101−4.
(35) Goyal, S.; Schutt, D. L.; Scoles, G. *Phys. Rev. Lett.* **1992**, *69*, 933−936.
(36) Hartmann, M.; Miller, R. E.; Toennies, J. P.; Vilesov, A. F. *Phys. Rev. Lett.* **1995**, *75*, 1566−1569.
(37) Moskun, A. C.; Jailaubekov, A. E.; Bradforth, S. E.; Tao, G.; Stratt, R. M. *Science* **2006**, *311*, 1907−1911.
(38) Lee, E.; Farrelly, D.; Whaley, K. B. *Phys. Rev. Lett.* **1999**, *83*, 3812−3815.
(39) Kwon, Y.; Huang, P.; Patel, M. V.; Blume, D.; Whaley, K. B. *J. Chem. Phys.* **2000**, *113*, 6469−6501.
(40) Paolini, S.; Fantoni, S.; Moroni, S.; Baroni, S. *J. Chem. Phys.* **2005**, *123*, 114306−1 − 114306−9.
(41) Xu, Y.; Jäger, W.; Tang, J.; McKellar, A. R. W. *Phys. Rev. Lett.* **2003**, *91*, 163401-1−163401-4.
(42) Tang, J.; Xu, Y. J.; McKellar, A. R. W.; Jäger, W. *Science* **2002**, *297*, 2030−2033.
(43) McKellar, A. R. W. *J. Chem. Phys.* **2006**, *125*, 164328-1−164328-8.
(44) Babichenko, V. S.; Kagan, Y. *Phys. Rev. Lett.* **1999**, *83*, 3458−3461.
(45) Zillich, R. E.; Kwon, Y.; Whaley, K. B. *Phys. Rev. Lett.* **2004**, *93*, 2504011−2504014.
(46) Tang, J.; McKellar, A. R. W.; Mezzacapo, F.; Moroni, S. *Phys. Rev. Lett.* **2004**, *92*, 145503-1−145503-4.
(47) Mikosz, A. A.; Ramilowski, J. A.; Farrelly, D. *J. Chem. Phys.* **2006**, *125*, 014312-1−014312-10.
(48) Holmgren, S. L.; Waldman, M.; Klemperer, W. *J. Chem. Phys.* **1977**, *67*, 4414−4422.
(49) Judd, B. R. *Operator Techniques in Atomic Spectroscopy*; McGraw-Hill: New York, 1963.
(50) Blume, D.; Lewerenz, M.; Kaloudis, M. *J. Chem. Phys.* **1996**, *105*, 8666−8683.
(51) Cazzato, P.; Paolini, S.; Moroni, S.; Baroni, S. *J. Chem. Phys.* **2004**, *120*, 9071−9076.
(52) Tang, J.; McKellar, A. R. W. *J. Chem. Phys.* **2003**, *119*, 754−764.
(53) Viel, A.; Whaley, K. B. *J. Chem. Phys.* **2001**, *115*, 10186−10198.
(54) Zillich, R. E.; Whaley, K. B. *Phys. Rev. B: Condens. Matter Mater. Phys.* **2004**, *69*, 104517-1−104517-21.
(55) Moszynski, R.; Wormer, P. E. S.; Jeziorski, B.; Avoird, A. *J. Chem. Phys.* **1994**, *101*, 2811−2824.
(56) Gui-Hua, S.; Xiang-Dong, Y.; Jun, Z.; Cai-Xia, W. *Chin. Phys.* **2002**, *11*, 910−914.
(57) Murdachaew, G.; Szalewicz, K.; Jiang, H.; Bacic, Z. *J. Chem. Phys.* **2004**, *121*, 11839−11855.
(58) Jiang, H.; Sarsa, A.; Murdachaew, G.; Szalewicz, K.; Bacic, Z. *J. Chem. Phys.* **2005**, *123*, 224313−224326.
(59) Fajin, J. L. C.; Fernandez, B.; Mikosz, A.; Farrelly, D. *Mol. Phys.* **2006**, *104*, 1413−1420.
(60) Aziz, R. A.; McCourt, F. R. W.; Wong, C. C. K. *Mol. Phys.* **1987**, *61*, 1487−1511.
(61) LeBlanc, R. B.; White, J. B.; Bernath, P. F. *J. Mol. Spect.* **1994**, *164*, 547−579.
(62) Herzberg, G. *Molecular spectra and molecular structure. I. Spectra of diatomic molecules*; D. van Nostrand Company, Inc.: Princeton, NJ, 1950.
(63) Boys, S. F.; Bernardi, F. *Mol. Phys.* **1970**, *19*, 553−566.
(64) Boys, S. F.; Bernardi, F. *Mol. Phys.* **2002**, *100*, 65−73 (reprinted).
(65) Bukowski, R.; Sadlej, J.; Jeziorski, B.; Jankowski, P.; Szalewicz, K.; Kucharski, S. A.; Williams, H. L.; Rice, B. M. *J. Chem. Phys.* **1999**, *110*, 3785−3803.
(66) Tang, K. T.; Toennies, J. P. *J. Chem. Phys.* **1984**, *80*, 3726−3741.
(67) Hutson, J. M. *Adv. Mol. Vibr. Coll. Dyn.* **1991**, *1A*, 1−45.
(68) Hutson, J. M. Bound, Version 5: A program for calculating bound-state energies for weakly BOUND molecular complexes, distributed via Collaborative Computing Project No. 6, of the Science and Engineering Research Council, on Molecular Quantum Dynamics; UK Technical report, 1993.
(69) Clary, D. C.; Nesbitt, D. J. *J. Chem. Phys.* **1989**, *90*, 7000−7013.
(70) Buch, V. *J. Chem. Phys.* **1992**, *97*, 726−729.
(71) Benoit, D. M.; Clary, D. C. *J. Chem. Phys.* **2000**, *113*, 5193−5202.
(72) Hammond, B. L.; Lester, W. A., Jr.; Reynolds, P. J. *Monte Carlo methods in ab initio quantum chemistry*; World Scientific: Singapore, 1994.
(73) Bressanini, D.; Reynolds, P. J. *Phys. Rev. Lett.* **2005**, *95*, 110201-1−110201-4.
(74) Viel, A.; Patel, M. V.; Niyaz, P.; Whaley, K. B. *Comp. Phys. Commun.* **2002**, *145*, 24−47.
(75) Nauta, K.; Miller, R. E. *J. Chem. Phys.* **2000**, *113*, 9466−9469.
(76) Hutson, J. M. *J. Chem. Phys.* **1990**, *92*, 157−168.
(77) Yutsis, A. P.; Levinson, I. B.; Vanagas, V. V. *Mathematical Apparatus of the Theory of Angular Momentum*; Israel Program for Scientific Translation: Jerusalem, Israel, 1962.
(78) Zare, R. N. *Angular Momentum: Understanding spatial aspects in chemistry and physics*; Wiley: New York, 1988.
(79) Varshalovich, D. A.; Moskalev, A. N.; Khersonskii, V. K. *Quantum Theory of Angular Momentum: Irreducible Tensors, Spherical Harmonics, Vector Coupling Coefficients, 3nj Symbols*; World Scientific: Singapore, 1988.